Negative parity states of ^{11}B and ^{11}C and the similarity with ^{12}C

Yoshiko Kanada-En'yo
Yukawa Institute for Theoretical Physics, Kyoto University, Kyoto 606-8502, Japan
(Received 2 November 2006; published 8 February 2007)

The negative parity states of ^{11}B and ^{11}C were studied based on the calculations of antisymmetrized molecular dynamics (AMD). The calculations reproduced well the experimental strengths of Gamov-Teller (GT), $M1$, and monopole transitions. We especially focused on the $3/2^-_3$ and $5/2^-_2$ states for which GT transition strengths were recently measured. The weak $M1$ and GT transitions for $3/2^-_3$ in ^{11}B and ^{11}C are described by a well-developed cluster structure of $2\alpha+t$ and $2\alpha+^3$He, respectively, while the strong transitions for $5/2^-_2$ is characterized by an intrinsic spin excitation with no cluster structure. It was found that the $3/2^-_3$ state is a dilute cluster state, and its features are similar to those of ^{12}C(0^+_2) which is considered to be a gas state of 3α clusters.

DOI: 10.1103/PhysRevC.75.024302 PACS number(s): 21.60.−n, 02.70.Ns, 21.10.Ky, 27.20.+n

I. INTRODUCTION

Cluster aspect is known to be an essential feature of light nuclei. Recently, various new types of cluster structures have been predicted and found in excited states of light stable nuclei as well as in light unstable nuclei. In the case of ^{12}C, it was known that 3α-cluster states develop in such excited states as the 0^+_2(7.65 MeV) state. Tohsaki *et al.* [1,2] proposed a new interpretation of the 0^+_2 as a dilute gas state of weakly interacting 3α particles. It is a challenging problem to determine whether such a cluster gas is a general feature that appears in other nuclear systems. To search for such dilute cluster states, we studied the structure of excited states of ^{11}C and ^{11}B.

The present study was motivated by recent measurements of Gamov-Teller (GT) transitions $^{11}\mathrm{B} \to {}^{11}\mathrm{C}^*$ with high energy resolutions [3,4]. In the experiments, the GT transition strengths to the $3/2^-_3$ and $5/2^-_2$ states were separately measured, and the transition to ^{11}C$(3/2^-_3, 8.10$ MeV) was found to be extremely weak compared with that to ^{11}C$(5/2^-_2, 8.42$ MeV) and also with those to other low-lying states. Abnormal features of the $3/2^-_3$ state have been known also in the mirror nucleus ^{11}B. For example, the $3/2^-_3$ state of ^{11}B has relatively weak $M1$ transitions into the lower states compared with the strong transitions among other low-lying states. Another characteristic of ^{11}B$(3/2^-_3)$ is the strong monopole transition observed by recent experiments on inelastic (d, d') scattering, where similarities of ^{11}B$(3/2^-_3)$ with ^{12}C(0^+_2) were suggested [5]. On the theoretical side, the structure of ^{11}B$(3/2^-_3)$ has been mysterious because this state cannot be described by any models. No theoretical state can be assigned to $3/2^-_3$ in shell-model [6–8] or cluster model calculations [9]. These facts indicate that the $3/2^-_3$ state of ^{11}B and ^{11}C may have an abnormal structure and is a candidate of the dilute cluster state. On the other hand, the shell models succeeded in reproducing various properties of low-lying negative parity states with the excitation energy $E_x < 9$ MeV except for $3/2^-_3$ [8]. This result suggests the possible coexistence of cluster states and noncluster states in ^{11}B and ^{11}C.

In this paper, we study the negative parity states of ^{11}B and ^{11}C based on theoretical calculations of antisymmetrized molecular dynamics (AMD). We apply the method of variation after spin-parity projections in the AMD framework, which has proved to be a powerful tool for studying excited states of light nuclei. We focus on the structures of the $3/2^-_3$ and $5/2^-_2$ states around $E_x = 8$ MeV and show the similarity of the excited states of ^{11}B with those of ^{12}C.

The paper is organized as follows. First, we briefly explain the theoretical method in Sec. II, and then we show the calculated results in comparison with the experimental data in Sec. III. In Sec. IV, we discuss the structures of excited states of ^{11}B and show their similarity with ^{12}C. Finally, we give a summary in Sec. V.

II. FORMULATION

We perform the energy variation after spin-parity projection (VAP) within the AMD model space, as was done in the previous studies [10,11]. The detailed formulation of the AMD method for nuclear structure studies is described in Refs. [10–14]. In particular, the formulation of the present calculations is basically the same as that described in Refs. [10,11,15].

An AMD wave function is a Slater determinant of Gaussian wave packets,

$$\Phi_{\mathrm{AMD}}(\mathbf{Z}) = \frac{1}{\sqrt{A!}}\mathcal{A}\{\varphi_1, \varphi_2, \ldots, \varphi_A\}, \tag{1}$$

where the i-th single-particle wave function is written by a product of spatial (ϕ), intrinsic spin (χ), and isospin (τ) wave functions as

$$\varphi_i = \phi_{\mathbf{X}_i}\chi_i\tau_i, \tag{2}$$

$$\phi_{\mathbf{X}_i}(\mathbf{r}_j) \propto \exp\left\{-\nu\left(\mathbf{r}_j - \frac{\mathbf{X}_i}{\sqrt{\nu}}\right)^2\right\}, \tag{3}$$

$$\chi_i = \left(\frac{1}{2} + \xi_i\right)\chi_\uparrow + \left(\frac{1}{2} - \xi_i\right)\chi_\downarrow. \tag{4}$$

ϕ and χ are represented by complex variational parameters, $\mathbf{X}_i$ and ξ_i. The isospin function τ_i is fixed to be up (proton) or down

(neutron). We use the fixed width parameter $\nu = 0.19$ fm^{-2}, which is chosen to be the optimum value for ^{11}B. Accordingly, an AMD wave function is expressed by a set of variational parameters, $\mathbf{Z} \equiv \{\mathbf{X}_1, \mathbf{X}_2, \ldots, \mathbf{X}_A, \xi_1, \xi_2, \ldots, \xi_A\}$.

For the lowest J^π state, we vary the parameters $\mathbf{X}_i$ and ξ_i $(i = 1 \sim A)$ to minimize the energy expectation value of the Hamiltonian $\langle\Phi|H|\Phi\rangle/\langle\Phi|\Phi\rangle$ for the spin-parity projected AMD wave function $\Phi = P^{J\pi}_{MK'}\Phi_{\rm AMD}(\mathbf{Z})$. Here, $P^{J\pi}_{MK'}$ is the spin-parity projection operator. Then we obtain the optimum solution of the parameter set: $\mathbf{Z}^{J\pi}_1$ for the lowest J^π state. The solution $\mathbf{Z}^{J\pi}_n$ for the n-th J^π state are calculated by varying $\mathbf{Z}$ so as to minimize the energy of the wave function, that is,

$$|\Phi\rangle = \left|P^{J\pi}_{MK'}\Phi_{\rm AMD}(\mathbf{Z})\right\rangle - \sum_{k=1}^{n-1}\left|P^{J\pi}_{MK'}\Phi_{\rm AMD}\left(\mathbf{Z}^{J\pi}_k\right)\right\rangle \times \frac{\left\langle P^{J\pi}_{MK'}\Phi_{\rm AMD}\left(\mathbf{Z}^{J\pi}_k\right)\middle|P^{J\pi}_{MK'}\Phi_{\rm AMD}(\mathbf{Z})\right\rangle}{\left\langle P^{J\pi}_{MK'}\Phi_{\rm AMD}\left(\mathbf{Z}^{J\pi}_k\right)\middle|P^{J\pi}_{MK'}\Phi_{\rm AMD}\left(\mathbf{Z}^{J\pi}_k\right)\right\rangle}, \quad (5)$$

which is the orthogonal component to the lower states.

After the VAP calculations of the J^π_n states for various J, n and $\pi = \pm$, we obtained the optimum intrinsic states, $\Phi_{\rm AMD}(\mathbf{Z}^{J\pi}_n)$, which approximately describe the corresponding J^π_n states. To improve the wave functions, we superpose all the obtained AMD wave functions. Namely, we determine the final wave functions for the J^π_n states as

$$\left|J^\pi_n\right\rangle = \sum_{i,K} c\left(J^\pi_n, i, K\right)\left|P^{J\pi}_{MK}\Phi_{\rm AMD}\left(\mathbf{Z}^{J_i\pi_i}_{k_i}\right)\right\rangle, \quad (6)$$

where the coefficients $c(J^\pi_n, i, K)$ are determined by the diagonalization of the Hamiltonian and norm matrices. Here the number of the independent AMD wave functions, which are superposed in Eq. (6), is that of the spin-parity states $\{J^\pi_n\}$ calculated by the VAP. We calculate the expectation values for various observables with the $|J^\pi_n\rangle$ obtained after diagonalization.

III. RESULTS

We adopt the same effective nuclear interaction as those used in Ref. [10], which consists of the central, spin-orbit, and Coulomb forces. The interaction parameters are slightly modified from the previous ones for better reproduction of the energy levels of ^{11}B and ^{11}C. Namely, the Bartlett, Heisenberg, and Majorana parameters in the MV1 force are chosen to be $b = h = 0.25$ and $m = 0.62$, and the strengths of the spin-orbit force are $u_I = -u_{II} = 2800$ MeV.

The base AMD wave functions are obtained by the VAP for the ground and excited states of ^{11}B. The number of the base AMD wave functions in the present calculations are 17. These independent AMD wave functions are superposed to calculate the final wave functions. In the calculations of ^{11}C, we assume the mirror symmetry of the base AMD wave functions for simplicity. The coefficients of the base wave functions in the superposition are optimized for each system of ^{11}B and ^{11}C.

The energy levels of the negative parity states in ^{11}B are shown in Fig. 1. In the results, we obtain the $3/2^-_3$ and $5/2^-_2$ states at about $E_x = 10$ MeV. We can assign the obtained $3/2^-_3$ and $5/2^-_2$ states to the observed $3/2^-_3$ ($E_x = 8.56$ MeV) and $5/2^-_2$ ($E_x = 8.92$ MeV) states because of the good agreements of transition strengths between theory and experimental data as shown later, though the excitation energies are overestimated by the present calculations.

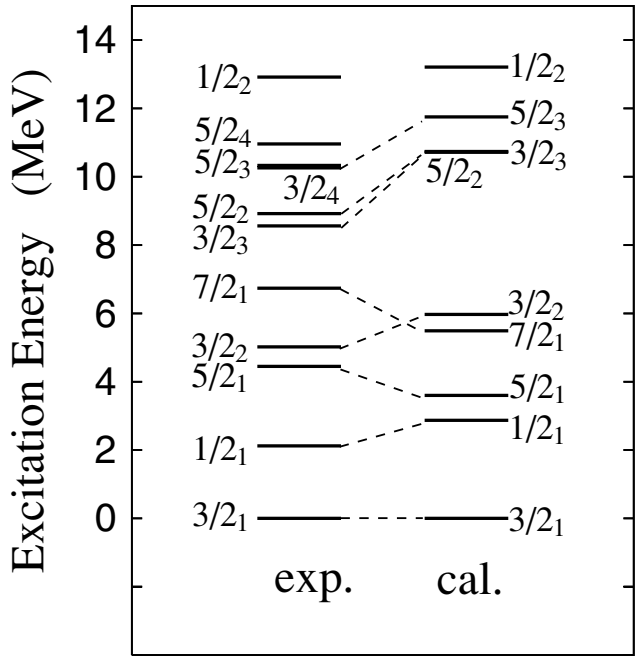

FIG. 1. Energy levels of the negative parity states of ^{11}B.

The GT transition strengths from ^{11}B$_{\rm g.s.}$ to ^{11}C* and the $M1$ and $E2$ transition strengths in ^{11}B are shown in Tables I, II, and III, respectively. The calculated values for these transitions are in good agreement with the observed values. The B(GT) for the transitions to ^{11}C$^*(3/2^-_3)$ and ^{11}C$^*(5/2^-_2)$ at $E_x \sim 8$ MeV were recently measured by charge exchange reactions [3,4], and it was found that $B(\mathrm{GT}; {}^{11}\mathrm{B} \to {}^{11}\mathrm{C}(3/2^-_3))$ is abnormally small, while $B(\mathrm{GT}; {}^{11}\mathrm{B} \to {}^{11}\mathrm{C}(5/2^-_2))$ is as large as those for other low-lying states of ^{11}C. The present result describes

TABLE I. Comparison of the GT transition strengths, binding energies (B.E.), Q moments, μ moments, and $2\alpha - t$ thresholds between present results and experimental data. Theoretical values obtained by the no-core shell model calculation with AV8'+TM'(99) [8] are also shown. Experimental data are from Ref. [4].

	Exp.	AMD	NCSM
$B(\mathrm{GT}; {}^{11}\mathrm{B} \to {}^{11}\mathrm{C}(3/2^-_1))$	0.345(8)	0.40	0.315
$B(\mathrm{GT}; {}^{11}\mathrm{B} \to {}^{11}\mathrm{C}(1/2^-_1))$	0.440(22)	0.43	0.591
$B(\mathrm{GT}; {}^{11}\mathrm{B} \to {}^{11}\mathrm{C}(5/2^-_1))$	0.526(27)	0.70	0.517
$B(\mathrm{GT}; {}^{11}\mathrm{B} \to {}^{11}\mathrm{C}(3/2^-_2))$	0.525(27)	0.67	0.741
$B(\mathrm{GT}; {}^{11}\mathrm{B} \to {}^{11}\mathrm{C}(3/2^-_3))$	0.005(2)	0.02	
$B(\mathrm{GT}; {}^{11}\mathrm{B} \to {}^{11}\mathrm{C}(5/2^-_2))$	0.461(23)	0.56	0.625
B.E.(^{11}B$_{\rm g.s.}$) (MeV)	76.205	72.8	73.338
$\mu(^{11}\mathrm{B}_{\rm g.s.})$ (μ_N^2)	+2.689	+2.3	+2.176
$Q(^{11}\mathrm{B}_{\rm g.s.})$ (e fm^2)	+4.065(26)	+4.7	+2.920
B.E.(^{11}C$_{\rm g.s.}$) (MeV)	73.440	70.4	70.618
$\mu(^{11}\mathrm{C}_{\rm g.s.})$ (μ_N^2)	−0.964	−0.6	−0.460
$Q(^{11}\mathrm{C}_{\rm g.s.})$ (e fm^2)	+3.327(24)	+3.8	+2.363
2α+t threshold (MeV)	65.07	70.6	

TABLE II. $M1$ transition strengths in ^{11}B. Theoretical values were calculated by the AMD (VAP) method.

J_i	J_f	$B(M1; J_i \to J_f)\,\mu_N^2$	
		Exp.	Theor.
$1/2^-_1$	$3/2^-_1$	1.07 (0.07)	1.2
$5/2^-_1$	$3/2^-_1$	0.52 (0.02)	0.72
$3/2^-_2$	$3/2^-_1$	1.13 (0.04)	1.2
$3/2^-_2$	$1/2^-_1$	0.98 (0.04)	1.0
$7/2^-_1$	$5/2^-_1$	0.006 (0.002)	0.03
$3/2^-_3$	$3/2^-_1$	0.072 (0.007)	0.07
$3/2^-_3$	$1/2^-_1$	0.091 (0.009)	0.16
$3/2^-_3$	$5/2^-_1$	0.057 (0.013)	0.04
$3/2^-_3$	$3/2^-_2$	0.163 (0.023)	0.28
$5/2^-_2$	$3/2^-_1$	0.50 (0.02)	0.45
$5/2^-_2$	$5/2^-_1$	0.21 (0.02)	0.04

well the small B(GT) for the $3/2^-_3$ state because it has a well-developed $2\alpha+^3$He cluster structure, and hence the structure of the daughter state differs greatly from the normal structure of the parent state, $^{11}B_{g.s.}$. For the same reason, the $M1$ transitions from ^{11}B$(3/2^-_3)$ to the low-lying states are generally weak compared with other $M1$ transitions among the low-lying states. On the other hand, since $5/2^-_2$ has no cluster structure, B(GT) for ^{11}C$^*(5/2^-_2)$ and $B(M1)$ for ^{11}B$^*(5/2^-_2)$ are as large as those for the other low-lying states in the theoretical results. This is consistent with the experimental data. We also show in Table I the theoretical B(GT) calculated by the no-core shell model (NCSM) [8]. The strengths of the GT transitions to ^{11}C* are reproduced also by the NCSM except for the transition to ^{11}C$^*(3/2^-_3)$. In the NCSM, the $3/2^-_3$ state cannot be described because the limited model space in the shell model is not suitable for describing cluster states with spatial development.

Recent experiments on inelastic (d, d') scattering [5] have found that the isoscalar monopole transition for $3/2^-_1 \to 3/2^-_3$ is as strong as $B(E0; IS) = 94 \pm 16$ fm^4. The calculated strength for this inelastic transition is $B(E0; IS) = 94$ fm^4, which agrees well with the experimental data.

TABLE III. Quadrupole transition strengths in ^{11}B. Present results of $B(E2)$, M_p, and M_n are shown with experimental values of $B(E2)$ [16].

J_i	J_f	Exp. $B(E2)$ (e^2 fm^4)	Theor. $B(E2)$ (e^2 fm^4)	M_p (e fm^2)	M_n (e fm^2)
$1/2^-_1$	$3/2^-_1$		4.5	3.0	4.0
$5/2^-_1$	$3/2^-_1$	14(3)	12.8	8.8	7.5
$3/2^-_2$	$3/2^-_1$		0.0	0.3	2.7
$7/2^-_1$	$3/2^-_1$	1.9(0.4)	1.8	3.8	7.9
$3/2^-_3$	$3/2^-_1$		0.8	1.8	2.8
$5/2^-_2$	$3/2^-_1$	1.0(0.7)	0.1	0.8	0.9
$5/2^-_3$	$3/2^-_1$		0.7	2.1	1.2

IV. DISCUSSIONS

In the present calculations of ^{11}B and ^{11}C, we found that the $3/2^-_3$ states are the well-developed three-center cluster states such as $2\alpha+t$ and $2\alpha+^3$He. We consider that these states are candidates for being cluster gas states, which are analogous to the 3α gas state proposed in ^{12}C(0^+_2). On the other hand, $5/2^-_2$ at almost the same excitation energy as $3/2^-_3$ is a noncluster state. In this section, we theoretically investigate the structure of ^{11}B while focusing on the cluster aspect, and we show the analogy of the excited states of ^{11}B with those of ^{12}C.

A. Intrinsic structure

As explained in Sec. II, by performing the VAP calculations, we obtained the optimum intrinsic states, $\Phi_{\rm AMD}(\mathbf{Z}_n^{J\pi})$. Although the final wave function $|J_n^\pi\rangle$ is expressed by the superposition of all the obtained AMD wave functions as Eq. (6), the spin-parity eigenstate $|P^{J\pi}_{MK}\Phi_{\rm AMD}(\mathbf{Z}_n^{J\pi})\rangle$ projected from the single AMD wave function is the dominant component of the $|J_n^\pi\rangle$ with an amplitude of more than 70% in most cases, except for $3/2^-_3$. In the case of $3/2^-_3$, since the amplitude is distributed into various AMD wave functions, the amplitude of the dominant component $|P^{3/2^-}_{MK}\Phi_{\rm AMD}(\mathbf{Z}_3^{3/2^-})\rangle$ in $|3/2^-_3\rangle$ is reduced to 50%. Here we regard the obtained $\Phi_{\rm AMD}(\mathbf{Z}_n^{J\pi})$ written by the single Slater determinant as the approximate intrinsic state of the corresponding J_n^π state, and discuss the intrinsic structure.

In Fig. 2, we display the density distribution of the excited states of ^{11}B. The matter density of the intrinsic wave functions $\Phi_{\rm AMD}(\mathbf{Z}_n^{J\pi})$ is also shown. As shown in the density, the ground state $(3/2^-_1)$ has no cluster structure, while the $3/2^-_2$ state has a structure with cluster cores. Since the spatial development of the clustering is not remarkable, the $3/2^-_2$ state is considered to be the SU(3)-limit cluster state. The most striking observation is that the spatially developed cluster structure of $2\alpha+t$ appears in the $3/2^-_3$ state. On the other hand, the $5/2^-_2$ state has no cluster structure, though this state appears at almost the same excitation energy as the $3/2^-_3$ state with the developed cluster structure. In a higher excited state, we found a somewhat linearlike $2\alpha+t$ cluster structure in $1/2^-_2$. The predicted $1/2^-_2$ state should be assigned to a $1/2^-$, $T = 1/2$ state; however, the corresponding state has not yet been observed.

Let us show similarities of the cluster features seen in the intrinsic structure of ^{11}B with those of ^{12}C. When we compare the present AMD results with those of ^{12}C in Ref. [15], we find a good correspondence of the intrinsic structure between ^{11}B and ^{12}C. As shown in Fig. 2, the ground states in both nuclei have no remarkable cluster structure because of the nature of the $p_{3/2}$ subshell closure. The cluster core structure in the ^{11}B$(3/2^-_2)$ state is similar to that of the ^{12}C(2^+_1). Both states show the three-center cluster core structure, but their spatial development is not remarkable. This means that ^{11}B$(3/2^-_2)$ and ^{12}C(2^+_1) can be practically dominated by the SU(3)-limit cluster states of $2\alpha+t$ and 3α, respectively. The spatially developed $2\alpha+t$ clustering in ^{11}B$(3/2^-_3)$ is similar to the developed 3α clustering in $C(0^+_2)$. The details are discussed later. The linearlike structure in ^{11}B$(1/2^-_2)$ is associated with that of the ^{12}C(0^+_3) and ^{12}C(1^-_1) states. Although the structure

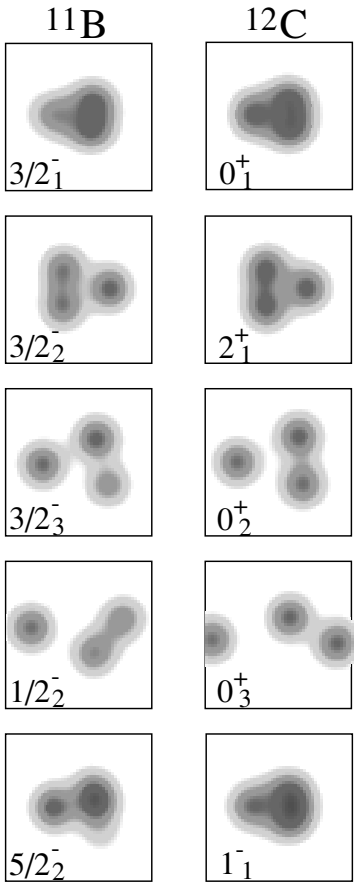

FIG. 2. Density distribution of ground and excited states in ^{11}B and ^{12}C, and density of the dominant AMD wave function of each state.

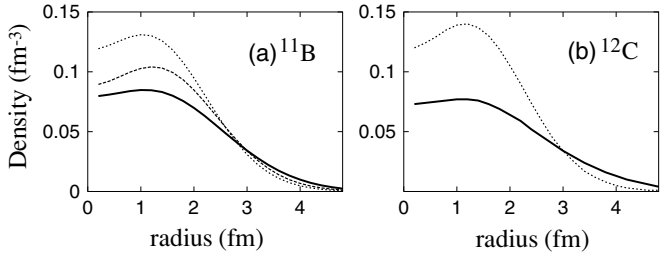

FIG. 3. Point matter density of (a) $3/2^-_1$ (dotted), $3/2^-_2$ (dashed), and $3/2^-_3$ (solid) states of ^{11}B, and (b) 0^+_1 (dotted) and 0^+_2 (solid) of ^{12}C.

of ^{12}C(0^+_3) is not yet experimentally and theoretically clarified, the linearlike 3α structure in ^{12}C was predicted by the generator coordinate method (GCM) calculation [17] and by fermionic molecular dynamics [18] as well as the AMD. The $5/2^-_2$ state has no cluster structure, because this state appears as a result of the intrinsic spin excitation, which causes the breaking of clusters. The situation is similar to the case of ^{12}C(1^+_1).

As mentioned before, the ^{11}C($3/2^-_3$, 8.10 MeV) and ^{11}B($3/2^-_3$, 8.65 MeV) states have abnormally small B(GT) and $B(M1)$ compared with other low-lying states in $E_x \leqslant 9$ MeV. The quenching of GT and $M1$ transitions for the $3/2^-_3$ states can be described by the above-mentioned exotic structure. Namely, since ^{11}C($3/2^-_3$) and $B(3/2^-_3)$ exhibit the well-developed 2α+^{3}He and $2\alpha+t$ clustering, they have a small transition overlap with the other normal low-lying states.

B. Dilute cluster states in $3/2^-_3$

By analyzing the obtained wave functions, we found that ^{11}B($3/2^-_3$) is a three-center cluster state with a spatially developed $2\alpha+t$ clustering. The clustering features of ^{11}B($3/2^-_3$) and ^{11}C($3/2^-_3$) are very similar to those of ^{12}C(0^+_2, 7.65 MeV), which is known to be a dilute gaslike 3α state. Therefore, we consider that ^{11}C($3/2^-_3$, 8.10 MeV) and ^{11}B($3/2^-_3$, 8.56 MeV) are candidates for dilute gaslike cluster states with 2α+^{3}He and $2\alpha+t$, respectively. The similarity between B($3/2^-_3$) and ^{12}C(0^+_2) has been suggested in Ref. [5], in which the experimental data of (d, d') scattering have been analyzed. We here theoretically discuss the similarity between ^{11}B($3/2^-_3$) and ^{12}C(0^+_2) by comparing the wave functions of ^{11}B and ^{12}C obtained by the same AMD as used in the present work [15].

To see the diluteness of the cluster states, first we plot the matter density $\rho(r)$ as a function of the radius r in Fig. 3. In the ground states of ^{11}B and ^{12}C, the density distributes in the small r region because of their compact structures. On the other hand, the density in the ^{11}B($3/2^-_3$) state is about half the normal density at the center and has a tail in the outer region because of the spatial development of clusters. The density curve of ^{11}B($3/2^-_3$) is similar to that of ^{12}C(0^+_2) though the outer tail is less remarkable than that of ^{12}C(0^+_2). Next we show the matter root-mean-square radii of the ground and excited states of ^{11}B and ^{12}C in Table IV. In ^{12}C, the 0^+_2

TABLE IV. Matter root-mean-square radii (r.m.s.r.) and expectation values of the harmonic oscillator quanta for protons (ΔQ_p) and neutrons (ΔQ_n). Values of ΔQ are defined by subtracting the minimum oscillator quanta. See details in text. Expectation values of the squared intrinsic spin for neutrons $\langle \mathbf{S}^2_n \rangle$ are also listed. The observed r.m.s.r. of the ^{12}C(0^+_1) is estimated to be 2.32–2.33 fm by the electron scattering data.

	r.m.s.r. (fm)	ΔQ_p	ΔQ_n	$\langle \mathbf{S}^2_n \rangle$
^{11}B($3/2^-_1$)	2.5	0.3	0.4	0.7
^{11}B($3/2^-_2$)	2.7	0.9	1.1	0.2
^{11}B($3/2^-_3$)	3.0	2.0	2.6	0.4
^{11}B($1/2^-_1$)	2.7	0.7	0.8	0.3
^{11}B($1/2^-_2$)	3.1	3.0	3.6	0.3
^{11}B($5/2^-_1$)	2.6	0.5	0.7	0.5
^{11}B($5/2^-_2$)	2.6	0.5	0.7	1.3
^{11}B($5/2^-_3$)	2.7	0.7	0.9	0.8
^{12}C(0^+_1)	2.5	0.4	0.4	0.6
^{12}C(0^+_2)	3.3	4.4	4.3	0.3
^{12}C(0^+_3)	4.0	10.0	9.9	0.1
^{12}C(2^+_1)	2.7	0.8	0.8	0.2
^{12}C(1^+_1)	2.5	0.2	0.2	1.4

state has a large radius. The calculated value of 0_2^+ is 3.3 fm in the AMD calculations, while those obtained by the RGM calculations [19] and the α condensate wave functions [2] are 3.5 and 3.8 fm, respectively. The smaller theoretical radius in the present method is considered to be caused by the limited number of base wave functions. In ^{11}B, the radius of the $3/2_3^-$ state is remarkably large compared with that of the ground state. Considering the large radius and the density tail in the outer region, we can say that the $3/2_3^-$ state exhibits the nature of a dilute cluster state.

To give a more quantitative discussion of the spatial development of clusters, we examine the expectation values of the harmonic oscillator (H.O.) quanta for protons and neutrons in Table IV. For the width parameters of the H.O., we use the same width of the Gaussian wave packets adopted in the AMD wave function. The values ΔQ are defined by subtracting the minimum oscillator quanta from the expectation values of the principal quantum number of H.O., namely,

$$\Delta Q \equiv \langle a^\dagger a \rangle - Q_{\min}, \tag{7}$$

where $Q_{\min}$ is 3(4) and 4(4) for protons(neutrons) of ^{11}B and ^{12}C, respectively. The expectation values of the oscillator quanta indicate the higher shell components in terms of the H.O. shell model. It is generally enhanced when the clustering spatially develops, because it necessarily increases the higher shell components. In ^{12}C(0_2^+) and ^{11}B$(3/2_3^-)$, the large ΔQ values are caused by the developed three-center cluster structure. Such higher shell components due to the cluster correlation in the developed cluster states cannot be treated in the truncated space of the shell model. This is why the shell-model calculations fail to describe the ^{12}C(0_2^+) and ^{11}B$(3/2_3^-)$ states. On the other hand, the ΔQ values in the ^{11}B$(3/2_2^-)$ are rather small compared with those of the $3/2_3^-$. It means that the major component of the $3/2_2^-$ is the $0\hbar\omega$ configuration. Since it has a compact state with cluster cores, as shown in Fig. 2, this state is interpreted to be almost the SU(3)-limit cluster state.

The similarity between the ^{11}B$(3/2_3^-)$ and ^{12}C(0_2^+) states has been suggested in Refs. [3,5], where the multipole decomposition analysis of the inelastic (d, d') scattering has been performed. The remarkable strengths of inelastic monopole transitions are the characteristics of these states. Figure 4 shows the calculated electron form factors for the monopole transitions ^{12}C$(0_1^+ \to 0_2^+)$, ^{11}B$(3/2_1^- \to 3/2_2^-)$, and ^{11}B$(3/2_1^- \to 3/2_3^-)$. The profile and absolute value of the form factor are similar for ^{11}B$(3/2_1^- \to 3/2_3^-)$ and ^{12}C$(0_1^+ \to 0_2^+)$, while the form factor for ^{11}B$(3/2_1^- \to 3/2_2^-)$ is more than a factor of 10^2 smaller. This is consistent with the experimental results of (d, d') scattering [3,5].

As mentioned above, we can see the developed cluster structure with dilute density in ^{11}B$(3/2_3^-)$ as well as ^{12}C(0_2^+). The ^{12}C(0_2^+) state is interpreted as a cluster gas state, where 3α clusters are moving rather freely [1,2]. Here "cluster gas" means the well-developed cluster state with dilute density, where the clusters are freely moving in terms of the weak coupling picture. Such a gaslike nature is reflected not only in the dilute density but also in the fragmentation of the amplitudes in the AMD model space. Let us remind the reader

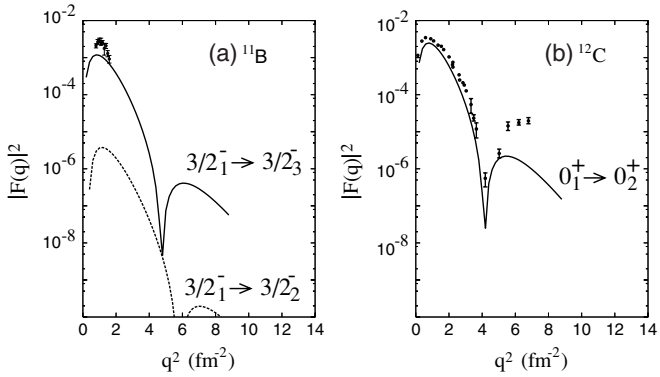

FIG. 4. Squared inelastic form factors for the electron scattering on (a) ^{11}B and (b) ^{12}C. The experimental form factors for the transitions to ^{11}B$(3/2^-, 8.56$ MeV) and ^{12}C(0_2^+) are taken from Refs. [20] and [21], respectively. Lines are calculated form factors of $E0$ components.

that a base AMD wave function is expressed by a Slater determinant. If the cluster state is written by an AMD wave function, it has a certain spatial configuration of the cluster centers like a single Brink-type cluster wave function [22]. On the contrary, when the state has a cluster gaslike feature, its wave function is written by a superposition of various AMD wave functions with different configurations of cluster centers. As a result, the cluster gas state is not dominated by a single AMD wave function, but the amplitudes distribute in various base wave functions. Actually, in ^{12}C(0_2^+), the amplitude of $|P^{0+}_{MK}\Phi_{\rm AMD}(\mathbf{Z}_2^{0+})\rangle$ is reduced to about 50% because of the cluster gas nature, as discussed in Ref. [15]. Similarly, in the case of ^{11}B$(3/2_3^-)$, the amplitude of the dominant component is only 50%, while those for ^{11}B$(3/2_1^-)$ and ^{11}B$(3/2_2^-)$ are more than 90%. This indicates the gaslike nature of the $2\alpha+t$ cluster in ^{11}B$(3/2_3^-)$ as well as the 3α cluster in ^{12}C(0_2^+).

Considering the smaller radius of ^{11}B$(3/2_3^-)$ than ^{12}C(0_2^+), the cluster gaslike nature in ^{11}B$(3/2_3^-)$ is not as remarkable as that in ^{12}C(0_2^+). We consider the reasons for the less gaslike nature in ^{11}B$(3/2_3^-)$ as follows. First, the intercluster potential is more attractive in the α-t channel than the α-α channel. This is already known in the comparison of the binding energy between ^{7}Li and ^{8}Be. The origin is that the repulsive Pauli effect is smaller in the α-t than the α-α. Second, from the natural extension of the ground state properties of ^{7}Li and ^{8}Be, it is expected that the triton motion may have the orbital angular-momentum $L = 1$, while the motion of the α clusters has $L = 0$. The $L = 1$ should be less favored to form a dilute cluster gas state than the $L = 0$. Third, it might be important that the symmetry of three clusters is not as good in the $2\alpha+t$ system as in the 3α system. Because of the symmetry of 3α orbits, the ^{12}C(0_2^+) state is understood as the α condensate state, as argued in Refs. [1,2,23,24]. However, it is not easy to define the bosonic behavior or to discuss the condensation in the $2\alpha+t$ system, which contains only two identical bosons.

In the stabilizing mechanism of dilute cluster states, one of the key factors preventing the states from shrinking is the orthogonality to the compact states in the lower energy

region. In both cases of ^{12}C and ^{11}B, there exist lower states with compact cluster components. In higher cluster states, the cluster distribution avoids the compact inner region and must spread out to satisfy the orthogonality to the lower states. It is interesting that the number of lower compact states is one (0^+_1) in ^{12}C and two ($3/2^-_1$, $3/2^-_2$) in ^{11}B, which is just the number of low-lying states described by the $0\hbar\omega$ configurations. This is why the dilute cluster state appears in the *third* $3/2^-$ state in the ^{11}B system.

The diluteness of the cluster states should be sensitive also to the relative energy against the threshold energy of the corresponding cluster channel. In the present results, the threshold energy for the three-body cluster breakup is not reproduced. To check the dependence of the structure of the excited states on the threshold energy, we varied the relative energy by changing the interaction parameters and found that the structure of the excited states are qualitatively unchanged. It means that the present results are not sensitive to the relative position of the threshold. It is because the present framework is a kind of bound state approximation. Since the number of base wave functions is limited, the long tail part of the intercluster motion may not be taken into account enough, and therefore the description of the detailed resonant behavior is insufficient in the present framework. In fact, the AMD calculations give a smaller radius for the ^{12}C(0^+_2) state than that obtained by the 3α cluster models. However, we should stress that the features of the 3α system obtained by the present method are qualitatively similar to those of the 3α-GCM calculations by Uegaki *et al*. [17]; they are also consistent with the 3α model of the orthogonal condition method (OCM) with the complex scaling method (CSM) [25], which treated the resonant behavior appropriately. This implies that the present results are useful for qualitative discussions, though the long tail part of the intercluster motion and its boundary conditions should be carefully treated for further quantitative study.

We should comment that the loosely bound cluster states have been predicted by Nishioka *et al*. with a $2\alpha+t$-OCM cluster model [9]. However, they could not assign the $3/2^-_3$ state because the reproduction of the energy spectra in the low-energy region was poor in the cluster model space.

C. Intrinsic spin excitation

In the ideal $2\alpha+t$ and 3α cluster states, the expectation values of the squared total intrinsic spin for neutrons $\langle \mathbf{S}^2_n \rangle$ should be zero, because spin-up and spin-down neutrons couple to become spin-zero pairs. In ^{11}B and ^{12}C, nonzero values of $\langle \mathbf{S}^2_n \rangle$ is caused by the component of the cluster breaking. We show the values of $\langle \mathbf{S}^2_n \rangle$ in ^{11}B and ^{12}C in Table IV. The $\langle \mathbf{S}^2_n \rangle$ values are small in cluster states such as ^{11}B($3/2^-_2$),^{11} B($3/2^-_3$), and ^{11}B($1/2^-_2$); while that of ^{11}B$_{\text{g.s.}}$ is $\langle \mathbf{S}_n \rangle^2 = 0.7$ and is as large as that of ^{12}C$_{\text{g.s.}}$ due to the component of the $p_{3/2}$ subshell closure. An interesting point is the large value, $\langle \mathbf{S}^2_n \rangle = 1.3$, in ^{11}B($5/2^-_2$). This means that the $5/2^-_2$ state is characterized by the intrinsic spin excitation of neutrons within the p shell. This feature corresponds well to the structure of ^{12}C(1^+_1), which is assigned to the observed 1^+_1(12.7 MeV) state. In the comparison of the experimental excitation energies between ^{11}B($5/2^-_2$) and ^{12}C(1^+_1) with the intrinsic spin excitation, it is interesting that ^{11}B($5/2^-_2$, 8.92 MeV) appears in the low-energy region and almost degenerates with the cluster gaslike ^{11}B($3/2^-_3$, 8.56 MeV), while ^{12}C(1^+_1, 12.7 MeV) exists at a much higher excitation energy than ^{12}C(0^+_2, 7.6 MeV). This implies that the intrinsic spin excitation more easily occurs in ^{11}B than in ^{12}C, and that the excitation energy of the intrinsic spin excitation is almost the same as that of the cluster excitation in ^{11}B.

V. SUMMARY

We studied the negative parity states in ^{11}B and ^{11}C based on the theoretical calculations of antisymmetrized molecular dynamics (AMD). It is concluded that various types of cluster states appear in the excited states of ^{11}B and ^{11}C. Recent experimental data of GT transition strengths for the $3/2^-_3$ and the $5/2^-_2$ states at $E_x \sim 8$ MeV are well reproduced by the cluster state and the noncluster state, respectively. It was found that the excitation energy of the intrinsic spin excitation is almost the same as that of the cluster excitation in ^{11}B. We compared the cluster aspect in the excited states of ^{11}B with that of ^{12}C and showed a good similarity between the $2\alpha+t$ and 3α systems.

We succeeded in describing the ^{11}B($3/2^-_3$, 8.56 MeV) and ^{11}C($3/2^-_3$, 8.10 MeV) states, which have not been reproduced by any other models. For the assignment of the theoretical states to the observed ones, it is essential to systematically describe the properties of the coexisting cluster and noncluster states in ^{11}C and ^{11}B. One of the new revelations in the present work is that ^{11}C($3/2^-_3$) and ^{11}B($3/2^-_3$) are the well-developed cluster states of $2\alpha+^3$He and $2\alpha+t$ with dilute density, respectively. The features of these dilute cluster states in ^{11}C and ^{11}B are similar to those of the 0^+_2 state of ^{12}C, which is understood to be a cluster gas of weakly interacting 3α particles.

Since the present framework is a kind of bound state approximation, the description of resonant behavior is not sufficient. The boundary conditions of the intercluster motion should be taken into account more carefully in more detailed investigations of the developed cluster states.

ACKNOWLEDGMENTS

The author would like to thank Prof. Schuck, Prof. Kawabata, and members of the Research Project for Study of Unstable Nuclei from Nuclear Cluster Aspects, sponsored by the Institute of Physical and Chemical Research (RIKEN), for many discussions. This work was partially performed under that project. The computational calculations in this work were performed by the Supercomputer Projects of High Energy Accelerator Research Organization (KEK) and also the supercomputers of YITP. This work was supported by the Japan Society for the Promotion of Science, and a Grant-in-Aid for Scientific Research of the Japan Ministry of Education, Science and Culture.

[1] A. Tohsaki, H. Horiuchi, P. Schuck, and G. Röpke, Phys. Rev. Lett. **87**, 192501 (2001).
[2] Y. Funaki, A. Tohsaki, H. Horiuchi, P. Schuck, and G. Röpke, Phys. Rev. C **67**, 051306(R) (2003).
[3] T. Kawabata *et al*., Phys. Rev. C **70**, 034318 (2004).
[4] Y. Fujita *et al*., Phys. Rev. C **70**, 011306(R) (2004).
[5] T. Kawabata *et al*., nucl-ex/0512040; Phys. Lett. B (in press).
[6] S. Cohen and D. Kurath, Nucl. Phys. **73**, 1 (1965).
[7] J. M. G. Gomez, J. C. Perez Cerdan, and C. Prieto, Nucl. Phys. **A551**, 451 (1993).
[8] P. Navratil and W. E. Ormand, Phys. Rev. C **68**, 034305 (2003).
[9] H. Nishioka, S. Saito, and M. Yasuno, Prog. Theor. Phys. **62**, 424 (1979).
[10] Y. Kanada-En'yo, Phys. Rev. Lett. **81**, 5291 (1998).
[11] Y. Kanada-En'yo, H. Horiuchi, and A. Doté, Phys. Rev. C **60**, 064304 (1999).
[12] Y. Kanada-En'yo, H. Horiuchi, and A. Ono, Phys. Rev. C **52**, 628 (1995); Y. Kanada-En'yo and H. Horiuchi, *ibid*. **52**, 647 (1995).
[13] Y. Kanada-En'yo and H. Horiuchi, Suppl. Prog. Theor. Phys. **142**, 205 (2001).
[14] Y. Kanada-En'yo, M. Kimura, and H. Horiuchi, C. R. Phys. **4**, 497 (2003).
[15] Y. Kanada-En'yo, nucl-th/0605047.
[16] F. Ajzenberg-Selove, Nucl. Phys. **A506**, 1 (1990).
[17] E. Uegaki, S. Okabe, Y. Abe, and H. Tanaka, Prog. Theor. Phys. **57**, 1262 (1977); E. Uegaki, Y. Abe, S. Okabe, and H. Tanaka, *ibid*. **59**, 1031 (1978); **62**, 1621 (1979).
[18] T. Neff and H. Feldmeier, Nucl. Phys. **A738**, 357 (2004).
[19] Y. Fukushima and M. Kamimura, J. Phys. Soc. Jpn. **44**, 225 (1978); M. Kamimura, Nucl. Phys. **A351**, 456 (1981).
[20] V. N. Polishchuk, N. G. Shevchenko, N. G. Afanasev, A. Y. Buki, A. A. Khomich, Yad. Fiz. **29**, 582 (1979).
[21] I. Sick and J. S. McCarthy, Nucl. Phys. **A150**, 631 (1970); A. Nakada, Y. Torizuka, and Y. Horikawa, Phys. Rev. Lett. **27**, 745 (1971); **27**, 1102(E) (1971); P. Strehl and Th. H. Schucan, Phys. Lett. **B27**, 641 (1968).
[22] D. M. Brink, in *Proceedings of the International School of Physics "Enrico Fermi,"* Varenna, 1965, Course 36, edited by C. Bloch (Academic Press, New York, 1966).
[23] T. Yamada and P. Schuck, Phys. Rev. C **69**, 024309 (2004).
[24] H. Matsumura and Y. Suzuki, Nucl. Phys. **A739**, 238 (2004).
[25] C. Kurokawa and K. Kato, Nucl. Phys. **A738**, 455 (2004).